# *miR-100 and miR-125b* Contribute to Enhanced Growth and Invasiveness

Hannah M. Nelson, Sherman Qu, Sydney N. Chapman, Nicole L. Luthcke, Sara A. Schuster, Lauren A. Turnbull, Muhammad Shameer, Lucas L. Guy, Xiao Lu, Kevin C. Corn, Kasey C. Vickers, Qi Liu, Jeffery L. Franklin, Allissa M. Weaver, Marjan Rafat, Robert J. Coffey, James G. Patton[#]

Department of Biological Sciences, Department of Cell and Developmental Biology, Department of Biomedical Engineering, Department of Pathology, Microbiology and Immunology, Department of Medicine, Center for Extracellular Vesicle Research, Vanderbilt University and Vanderbilt University Medical Center, Nashville TN

[#]Corresponding Author:

James G Patton

Department of Biological Sciences, Vanderbilt University

james.g.patton@vanderbilt.edu

**Abstract**

Extracellular communication via the transfer of vesicles and nanoparticles is now recognized to play an important role in tumor microenvironment interactions. Colorectal cancer (CRC) cells upregulate and secrete abundant levels of *miR-100 and miR-125b* that can alter gene expression by cell- and non-cell-autonomous mechanisms. We previously showed that these miRNAs activate Wnt signaling through noncanonical pairing with 5 negative regulators of Wnt signaling. To identify additional targets of *miR-100 and miR-125b*, we used bioinformatic approaches comparing multiple CRC cell lines, including knockout lines lacking one or both miRNAs. From an initial list of 117 potential mRNA targets of *miR-100 and miR-125b*, we validated 8 targets including Cingulin, a protein that links the cytoskeleton to tight junctions and modulates epithelial to mesenchymal transition (EMT). Here, we show that *miR-100 and miR-125b* can be transferred between cells to silence target mRNAs. We also show that these miRNAs contribute to enhanced 3D growth and invasiveness.

**Introduction**

MicroRNAs (miRNAs) are small (22-23nt) RNAs that base pair with target mRNAs to regulate gene expression by decreasing translation and promoting RNA degradation (He and Hannon 2004; Krol et al. 2010). In cancer, miRNA expression patterns are frequently altered contributing to all aspects of tumor progression from proliferation to metastasis (Peng and Croce 2016). We and others have focused on the role of *miR-100 and miR-125b* in cancer (Cha et al. 2015; Qin et al. 2015; Lu et al. 2017; Peng et al. 2021; Liu et al. 2022). These miRNAs and *let-7a-2* are encoded in the

third intron of *MIR100HG*, a 3kb lncRNA that is encoded as part of the large 300kb MIR100HG locus (Emmrich et al. 2014). Increased expression of *miR-100, miR-125 and MIR100HG* can promote cetuximab resistance in colorectal cancer cells, drive progression of pancreatic cancer, and promote epithelial to mesenchymal transition (Lu et al. 2017; Ottaviani et al. 2018; Liu et al. 2022). These effects are driven in part by regulating the expression of target mRNAs including mTOR (Cha et al. 2015), 5 negative regulators of Wnt signaling (Lu et al. 2017), CTFR and CGN (Zhang et al. 2021), and checkpoint kinases (CHK) (Ottaviani et al. 2018).

Extracellular vesicles (EVs) and nanoparticles are now recognized to play an important role in cell-cell communication through the transfer of RNA, protein and lipids (Couch et al. 2021; Dixson et al. 2023). Among RNA cargo, transfer of miRNA is the most well characterized due to their small size and ability to monitor silencing of targets in recipient cells (Valadi et al. 2007; Skog et al. 2008; Vickers et al. 2011). We previously showed that *miR-100 and miR-125b* are enriched in small EVs from colorectal cancer cells and Transwell co-culture experiments supported extracellular transfer of these miRNAs to recipient cells. Using cell lines containing CRISPR/Cas9 mediated knockouts of *miR-100 and miR-125b*, we demonstrate direct functional transfer of these miRNAs between cells. Further, we show that *miR-100 and miR-125b* contribute to enhanced 3D growth and invasiveness.

## Materials and Methods

### *Cell culture*

CC and CC-CR cells were obtained from the Coffey lab (Lu et al. 2017). All cell lines were confirmed to be free of mycoplasma contamination (Venor™GeM Mycoplasma Detection Kit, PCR-based, Sigma Aldrich Cat #MP0025). Cells were grown in Dulbecco's Modified Eagle's Medium (DMEM, Corning) supplemented with 10% fetal bovine serum (FBS, Corning), 1% L-glutamine (200 nM, Gibco), 1% MEM nonessential amino acids (Sigma Aldrich), and 1% penicillin-streptomycin (10,000 U/mL, Gibco) in 5% $CO_2$ at 37°C. Cells were passaged a maximum of 8 times before discarding.

*Generation of Knockout Cell Lines*

miR100 or miR125b or miR100/125b double knockout cell lines were generated by using multiplex CRISPR technology(Kabadi et al. 2014). Briefly, gRNAs flanking the targeted locus were designed based on Benching website. gRNA oligonucleotides were first cloned into intermediate sgRNA expression vectors (Addgene #53186-53189). Then multiple sgRNA expression cassettes were cloned into a lentiviral destination vector pLV hUbC-Cas9-T2A-GFP (Addgeene, #53190) by using Golden Gate assembly. Lentiviruses were made by co-transfecting 293T cells with resultant vector, pMD2.G and psPAX2 and used to transduce CCCR cells. Single GFP+ cells were sorted into 96 cell plates and expanded. The PCR primers located up and down stream of the gRNAs were used to identify the clones with desired homo-deletion *by using genomic DNA derived from expanded single GFP+ cells*.

*qRT-PCR*

Total RNA from both whole cell and sEVs were isolated using TRIzol (Life Technologies). Taqman small RNA assays (Life Technologies) were utilized to quantify miRNA levels. A total of 10ng of RNA were utilized for each RT reaction; 0.67 µl of cDNA was used in each 10µl qPCR reactions. qPCR was completed in either 96-well or 384-well plates on a Biorad CFX96 or CFX384 instruments. Fold changes were calculated as previously described (Cha et al. 2015).

*sEV Isolation*

Cells were plated at 9.0 x $10^6$ cells in T-175 flasks (Corning), with each sEV collection requiring 3 flasks. Cells were grown until 80% confluency, washed 3 times with sterilized 1X PBS, and media were replaced with DMEM lacking FBS and grown for 48 hours. Media were collected and cells were counted. Media was centrifuged at increasing speeds and time: 1,000xg for 10 minutes (room temperature), 2,000xg for 20 minutes (4°C), and 10,000xg for 30 minutes (4°C). A crude EV pellet was obtained after the conditioned media was centrifuged for 17 hours at 100,000xg (4°C). The pellet was washed two times by resuspending the pellet in 1mL of 1X DPBS (Corning) and centrifuged at 100,000xg for 70 minutes. Final pellets were resuspended in 100µl 1X DPBS. sEVs were quantified by protein concentration (Pierce BCA Protein Assay) and by nanoparticle tracking analysis (NTA, ZetaView Nanoparticle Tracking Analysis Instrument).

*Transfer assays*

For transwell assays, cells were plated in transwell plates (Corning, 3460) with 50,000 cells in the donor well and 300,000 cells in the recipient well. Transwell experiments were grown for five days, changing media every 72 hours. Recipient cells were washed 3 times with 2 mL of sterilized 1X PBS; RNA was then collected from either donor or recipient cells.

Cells were plated in a 12 well plate (Corning) with 100,000 cells per well. EVs were added to designated wells at 10ug of protein/mL of cell culture media. Cells were grown for five days, changing media every 48 hours.

*Ago-2 Immunoprecipitation*

Anti-Ago2, clone 11A9 antibody (MABE253, Sigma-Aldrich) and IgG. Ten 150cm dishes of  either CC or CC-CR cells were grown to 95% confluency. Cells were then scraped in ice cold PBS and centrifuged to collect the cell pellet in ice cold lysis buffer ( 20mM Tris HCl pH 7.5, 150 mM KCl, 0.5% NP40, 2mM EDTA, 1mM NaF, 0.5mM DTT, protease and RNAse inhibitors). Cell lysates were then incubated with rotation with Dynabeads. Prior to cell lysis, Dynabeads™ Protein G (ThermoFisher, 10003D) were prepped and conjugated with antibody overnight at 4°C and washed two times with ice cold lysis buffer. Cell lysates were then added to the conjugated beads and incubated at 4°C for six hours. Beads were gently washed and proteins were eluted. For RNA isolation, beads were incubated with DNAse and Proteinase K for 10 minutes at room temperature. Trizol was then added and incubated at room temp for 10 minutes. The following RNA product was isolated using a Trizol extraction.

*Small RNA sequencing (sRNA-seq)*

sRNA libraries were generated using the NEXTFlex Small RNA Library Preparation Kits v3 (Perkin) with the following modifications: (1) 3′- and 5′-adaptors were diluted 1:8, (2) 3′-adaptor ligations were performed overnight in multiple steps – 25°C for 2 h, 20°C for 4 h and 16°C overnight, (3) following cDNA synthesis and before barcoding PCR, step F protocol was followed, and (4) PCR amplification was 20 cycles. Following PCR amplification, individual libraries were size-selected (136–200 bp product) using Pippin Prep (Sage Sciences). Size-selected libraries were quantified using Qubit Fluorometer. Libraries were checked for quality and sequenced using Illumina short-read technology. Libraries were pooled and paired-end sequencing (PE-150) of the pool (equimolar multiplexed libraries) was performed on the NovaSeq6000 platform by the VANTAGE core (Vanderbilt University). Demultiplexing and bioinformatic analyses was performed using the TIGER pipeline (Allen et al. 2018). Briefly, Cutadapt (v1.16) was used to trim 3′ adaptors and all reads with < 16 nucleotides (nts) were removed (Martin 2011). Quality control on both raw reads and adaptor-trimmed reads was performed using FastQC (v0.11.9)(www.bioinformatics.babraham.ac.uk/projects/fastqc). The adaptor-trimmed reads were mapped to the hg19 genome, with additional rRNA and tRNA reference sequences, by Bowtie1 (v1.1.2) allowing only one mismatch (Langmead and Salzberg 2012).

*Total RNA Sequencing*

Bulk RNA sequencing libraries were prepared using Universal RNAseq kits (Tecan), as per manufacturer's instructions. Libraries were cleaned (Zymo), checked for quality using the Agilent bioanalyzer, quantified (Qubit), and pooled based on equimolar concentrations of libraries. Pooled libraries were sequenced using Illumina short-read technology based on PE150 on the NovaSeq6000 (Illumina). After sequencing, samples (libraries) were demultiplexed and analyzed. Briefly, reads were trimmed to remove adapter sequences using Cutadapt v2.10)(Martin 2011) and aligned to the Gencode GRCh38.p13 genome using STAR (v2.7.8a)(Dobin et al. 2013). Gencode v38 gene annotations were provided to STAR to improve the accuracy of mapping. Quality control on both raw reads and adaptor-trimmed reads was performed using FastQC (v0.11.9). FeatureCounts (v2.0.2)(Liao et al. 2014) was used to count the number of mapped reads to each gene. Heatmap3 (Zhao et al. 2014) was used for cluster analysis and visualization. Significant differential expressed genes with absolute fold change > 2 or < 0.5, and adjusted p value (padj) < 0.05 were determined using DESeq2 (v1.30.1)(Love et al. 2014). Genome Ontology and KEGG pathway over-representation analyses were performed on differentially expressed genes using the WebGestaltR package (NULL)(Wang et al. 2017). Gene set enrichment analysis (GSEA) was performed using GSEA package (v4.3.2)(Subramanian et al. 2005) on database v2022.1.Hs.

*Gene Expression Analysis*

The GENT2 Gene Expression database of Normal and Tumor tissues was used to compare levels of expression between 72 paired normal and tumor tissues utilizing the

GPL570 platform. Utilizing the 'Gene Profile' section of the database, gene expression patterns were documented throughout the various tissue samples. Statistical significance was determine using two-sample t-tests [GPL570 platform (HG-U133_Plus_2)].

*Luciferase Plasmid generation*

Short segments of the 3'UTR of mRNA of interests were cloned using RT/PCR into pMIR-REPORT™ miRNA Expression Reporter Vector System using NEBuilder HiFi DNA Assembly (New England BioLabs). PCR amplification primers are described in the Supplement. All plasmids were verified by sequencing (Genewiz).

*Luciferase Assay*

For luciferase assays, cells were grown to 60% confluency then transfected with Renilla vector (0.5ug DNA/mL) and luciferase constructs (1ug DNA/mL) using TransIT®-2020 (Mirus, MIR5404) for 72 hours. Cells were then washed and the Dual-Glo® Luciferase Assay System (Promega) was utilized according to manufacturer's instructions. Changes in luciferase levels were normalized to Renilla levels. For functional transfer of miRNAs utilizing luciferase assays, cells were co-cultured in Transwells.

**Results**

We previously reported that *miR-100 and miR-125* are significantly upregulated in colorectal cancer cells that are resistant to the cetuximab, a monoclonal antibody that targets the epidermal growth factor receptor (EGFR)(Lu et al. 2017). Increased Wnt

signaling in cetuximab resistant cells was consistent with silencing of 5 negative regulators of the Wnt pathway by *miR-100 and miR-125b* (Lu et al. 2017). However, these Wnt targets were noncanonical miRNA targets. Base pairing between miRNAs and 3'-UTR elements in mRNA targets is imperfect, but thought to be heavily driven by extensive pairing between nucleotides 2-8 of the miRNA (the "seed" sequence) (Bartel 2009). Because the extent of base pairing between miRNAs and their mRNA targets is highly variable, even within the seed sequence, identification of *bona fide* mRNA targets is a challenge (Li et al. 2008). Another challenge for miRNA function is to demonstrate extracellular transfer with direct silencing of mRNA targets in recipient cells (Gruner and McManus 2021). To address these challenges, we used CRISPR/Cas9 technology to generate cell lines with deletions of *miR-100, miR-125b* or both (**Supp. Fig. 1**). These lines were generated in the parental CC-CR cell line to provide tools to identify differentially expressed genes comparing cells overexpressing *miR-100 and miR-125b* to knockout lines thereby facilitating identification of mRNA targets for these miRNAs and for use in extracellular transfer experiments. As shown in **Fig. 1**, our CRISPR/Cas9 targeting strategy generated cell lines with undetectable levels of *miR-100 and miR-125b*.

**Identification of mRNA targets of *miR-100 and miR125b***

RNAseq was performed on our knockout lines (Δ*miR-100*, Δ*miR-125b*, and Δ*miR-100/miR-125b*) and bioinformatic analyses were performed to identify mRNA targets for *miR-100 and miR-125b* (**Supp. Table 1**). Initially, a three step bioinformatic analysis was conducted (**Fig. 2A)** to identify potential targets that are upregulated in CC

cells in comparison to CC-CR, are upregulated in the knockout lines compared to CC-CR cells, and are also putative targets prediction algorithms. This analysis resulted in the identification of 45 potential targets for *miR-100* and 35 potential targets for *miR-125b* (**Fig. 2B**).

Silencing of mRNAs by miRNA occurs in the RNA Induced Silencing Complex (RISC) containing one or more members of the Argonaute family (Liu et al. 2004; Farazi et al. 2008; Cenik and Zamore 2011; Müller et al. 2020). To enrich for targets of *miR-100 and miR-125b* in CC-CR cells, we performed RNA immunoprecipitation of AGO2 followed by short and long RNA sequencing (**Supp. Table 2, 3**). This allowed for the identification of an additional 37 targets of *miR-100 and miR-125b* (**Fig. 2C,D; Supp. Fig. 3).**

**Silencing of mRNA targets of miR-100 and miR-125b**

We next generated three different categories of luciferase vectors to test silencing of candidate mRNAs by *miR-100 and miR-125b* (**Fig. 3A**). Vectors were created that either have no target 3'UTR fused to the luciferase open reading frame; perfect 3'-UTR binding sites for *miR-100 or miR-125b*, or fusion of candidate gene 3'UTRs to the luciferase open reading frame. Vectors were transfected into CC-CR cells or the knockout lines and luciferase levels were determined (**Fig. 3B**). Several mRNA targets were shown to be targeted by *miR-100 and miR-125b* through rescue of luciferase activity in the knockout cells, with Cingulin (CGN) and Protein tyrosine phosphatase receptor type-R (PTPRR) being the most significant targets (**Fig. 3B**; **Supp. Fig. 4**).

**Cingulin and PTPRR are down regulated in colorectal cancer**

In 3D culture conditions in collagen, CC-CR form solid, disorganized colonies, indicative of aggressive behavior (Lu et al. 2017). Since *miR-100 and miR-125b* are overexpressed in CC-CR cells, the prediction is that cancer cells should show decreased expression of Cingulin and PTPRR. To test this, we used the GENT2 database to compare the levels of Cingulin and PTPRR between normal and cancer tissues (**Fig. 4A,B**). This analysis revealed that not only in colorectal cancer samples are CGN and PTPRR downregulated, but also across a variety of cancers. This supports the importance of *miR-100 and miR-125b* and regulation of their targets in cancer.

**Extracellular Transfer of *miR-100 and miR-125b***

Using our knockout lines as recipient cells allowed us to test for transfer of *miR-100 and miR-125b*. We used CC-CR cells as donor cells in Transwell co-culture experiments because EVs from CC-CR cells are enriched for *miR-100 and miR-125b* (**Fig. 5A).** We observed a significant increase in *miR-100 and miR-125b* levels when Δ*miR-100/miR-125b* recipient cells were co-cultured with CC-CR cells (**Fig. 5B**).

We also used our knockout lines to test silencing of mRNA targets of *miR-100 and miR-125b*. For this, Δ*miR-100/miR-125b* cells were transfected with luciferase constructs containing 3'UTRs from control, Cingulin, and PTPRR (**Fig. 5C**). Consistent with the luciferase assays in Fig. 3, we found that luminescence from the Cingulin and PTPRR luciferase constructs were significantly reduced when expressed in Δ*miR-*

*100/miR-125b* cells (**Fig. 5D**). This is the first evidence that *miR-100 and miR-125b* can functionally transfer from one cell to another.

**Transfer of *miR-100 and miR125b* Targets Cingulin**

Cingulin connects tight junctions to the cytoskeleton, bridging proteins such as ZO-1 (Citi et al. 1988; Zhang et al. 2021). Immunofluorescence revealed that in cells that had little or no detectable expression of *miR-100 or miR-125b* (CC and Δ*miR-100/miR-125b*), CGN expression was readily detected and localized to cell-cell junctions (**Fig. 6A**). However, in cells with high levels of *miR-100 and miR-125b*, CGN expression was undetectable (**Fig. 6A**). These data support targeting of Cingulin by *miR-100 and miR-125b,*

To test where extracellular transfer of miR-100 and miR-125b could downregulate cingulin, we used Transwell experiments with CC-CR donor cells and Δ*miR-100/miR-125b* recipient cells. After co-culture, we performed immunofluorescence on recipient cells using antibodies against Cingulin **(Fig. 6B**). When CC-CR cells were used as the donor, we observed reduced Cingulin levels compared to Δ*miR-100/miR-125b* donor cells (**Fig. 6B**). This indicates that Cingulin protein levels are downregulated by transfer of *miR-100 and miR-125b*.

***miR-100 and miR-125b* Contribute to Enhanced 3D Growth and Invasiveness in Recipient Cells**

Loss of CGN has been shown to increase invasiveness, metastatic potential and EMT (Guillemot and Citi 2006; Mangan et al. 2016; Schossleitner et al. 2016). To test the effect of the loss of *miR-100 and miR-125b* on 3D growth, we used spheroid cultures conditions. Under these conditions, the morphology of the Δ*miR-100/miR-125b* cell line appeared more similar to CC cells as opposed to the parental CC-CR cell line (**Supp. Movies 1-3**). After 5 days, we also observed changes in the dynamics of the colony surfaces when comparing the different cell lines. Increased projections emanating from the edges of the colony were observed in CC-CR cells with far fewer projections in CC cells grown under the same conditions (**Fig. 7A**). The Δ*miR-100/miR-125b* cell line was more similar to projections observed with CC cells. Quantification of overall spheroid growth revealed that cells expressing high levels of *miR-100 and miR-125b* cells (CC-CR) showed a significant increase in area when compared to low expressing (CC) or Δ*miR-100/miR-125b* cells (**Fig. 7B**). Lastly, we quantified an overall invasiveness potential by determining the increase in projection surface area after growth in collagen for five days (**Fig. 7C**). CC-CR showed a significantly greater projection area increase compared to CC and Δ*miR-100/miR-125b* cells, supporting that high levels of *miR-100 and miR-125b* can promote invasion.

## Discussion

Most studies examining transfer of miRNA by EVs face the challenge of demonstrating direct targeting of transcripts in recipient cells because the recipient cells also express the miRNA of interest (Gruner and McManus 2021). In these cases, it is possible that silencing of target mRNAs could be due to indirect mechanisms. Our

knockout cell lines provided an essential control to definitively demonstrate transfer of *miR-100 and miR-125b*.

We also used our knockout lines, Ago2 immunoprecipitation, and RNAseq to identify differentially expressed genes comparing high and low expression of *miR-100 and miR-125b*. Bioinformatic analyses of the RNAseq data set allowed for the identification of mRNA target of these miRNAs which we then validated using luciferase assays and immunofluorescent staining of Cingulin.

Lastly, using 3D spheroid growth conditions, we show that *miR-100 and miR-125b* contribute to enhanced 3D growth and invasiveness. This is consistent with gene expression analyses comparing normal and cancer cells which showed that decreased levels of two targets of miR-100 and miR125b (Cingulin and PTPRR) are observed in cancer.

## References


Allen RM, Zhao S, Ramirez Solano MA, Zhu W, Michell DL, Wang Y, Shyr Y, Sethupathy P, Linton MF, Graf GA et al. 2018. Bioinformatic analysis of endogenous and exogenous small RNAs on lipoproteins. *Journal of extracellular vesicles* **7**: 1506198.

Bartel DP. 2009. MicroRNAs: target recognition and regulatory functions. *Cell* **136**: 215-233.

Cenik ES, Zamore PD. 2011. Argonaute proteins. *Curr Biol* **21**: R446-449.

Cha DJ, Franklin JL, Dou Y, Liu Q, Higginbotham JN, Beckler MD, Weaver AM, Vickers K, Prasad N, Levy S et al. 2015. KRAS-dependent sorting of miRNA to exosomes. *eLife* **4**: e07197.

Citi S, Sabanay H, Jakes R, Geiger B, Kendrick-Jones J. 1988. Cingulin, a new peripheral component of tight junctions. *Nature* **333**: 272-276.

Couch Y, Buzas EI, Di Vizio D, Gho YS, Harrison P, Hill AF, Lotvall J, Raposo G, Stahl PD, Thery C et al. 2021. A brief history of nearly EV-erything - The rise and rise of extracellular vesicles. *Journal of extracellular vesicles* **10**: e12144.

Dixson AC, Dawson TR, Di Vizio D, Weaver AM. 2023. Context-specific regulation of extracellular vesicle biogenesis and cargo selection. *Nat Rev Mol Cell Biol*.

Dobin A, Davis CA, Schlesinger F, Drenkow J, Zaleski C, Jha S, Batut P, Chaisson M, Gingeras TR. 2013. STAR: ultrafast universal RNA-seq aligner. *Bioinformatics* **29**: 15-21.

Emmrich S, Streltsov A, Schmidt F, Thangapandi VR, Reinhardt D, Klusmann JH. 2014. LincRNAs MONC and MIR100HG act as oncogenes in acute megakaryoblastic leukemia. *Mol Cancer* **13**: 171.

Farazi TA, Juranek SA, Tuschl T. 2008. The growing catalog of small RNAs and their association with distinct Argonaute/Piwi family members. *Development* **135**: 1201-1214.

Gruner HN, McManus MT. 2021. Examining the evidence for extracellular RNA function in mammals. *Nat Rev Genet* **22**: 448-458.

Guillemot L, Citi S. 2006. Cingulin regulates claudin-2 expression and cell proliferation through the small GTPase RhoA. *Mol Biol Cell* **17**: 3569-3577.

He L, Hannon GJ. 2004. MicroRNAs: small RNAs with a big role in gene regulation. *Nat Rev Genet* **5**: 522-531.

Kabadi AM, Ousterout DG, Hilton IB, Gersbach CA. 2014. Multiplex CRISPR/Cas9-based genome engineering from a single lentiviral vector. *Nucleic Acids Res* **42**: e147.

Krol J, Loedige I, Filipowicz W. 2010. The widespread regulation of microRNA biogenesis, function and decay. *Nat Rev Genet* **11**: 597-610.

Langmead B, Salzberg SL. 2012. Fast gapped-read alignment with Bowtie 2. *Nat Methods* **9**: 357-359.

Li N, Flynt A, Kim HR, Solnica-Krezel L, Patton J. 2008. Dispatched Homolog 2 is targeted by miR-214 through a combination of three weak microRNA recognition sites. *Nucleic Acids Res* **36**: 4277-4285.

Liao Y, Smyth GK, Shi W. 2014. featureCounts: an efficient general purpose program for assigning sequence reads to genomic features. *Bioinformatics* **30**: 923-930.

Liu H, Li D, Sun L, Qin H, Fan A, Meng L, Graves-Deal R, Glass SE, Franklin JL, Liu Q et al. 2022. Interaction of lncRNA MIR100HG with hnRNPA2B1 facilitates m(6)A-dependent stabilization of TCF7L2 mRNA and colorectal cancer progression. *Mol Cancer* **21**: 74.

Liu J, Carmell MA, Rivas FV, Marsden CG, Thomson JM, Song JJ, Hammond SM, Joshua-Tor L, Hannon GJ. 2004. Argonaute2 is the catalytic engine of mammalian RNAi. *Science* **305**: 1437-1441.

Love MI, Huber W, Anders S. 2014. Moderated estimation of fold change and dispersion for RNA-seq data with DESeq2. *Genome Biol* **15**: 550.

Lu Y, Zhao X, Liu Q, Li C, Graves-Deal R, Cao Z, Singh, B., Franklin JL, Wang J, Hu H, Yang M et al. 2017. lncRNA MIR100HG-derived miR-100 and miR-125b mediate Cetuximab resistance via Wnt/beta catenin signaling. *Nature Medicine* **23**: 1331-1341.

Mangan AJ, Sietsema DV, Li D, Moore JK, Citi S, Prekeris R. 2016. Cingulin and actin mediate midbody-dependent apical lumen formation during polarization of epithelial cells. *Nature communications* **7**: 12426.

Martin M. 2011. Cutadapt removes adapator sequences from high-throughput sequencing reads. *EMBnetjournal* **17**: 10-12.

Müller M, Fazi F, Ciaudo C. 2020. Argonaute Proteins: From Structure to Function in Development and Pathological Cell Fate Determination. *Frontiers in Cell and Developmental Biology* **7**.

Ottaviani S, Stebbing J, Frampton AE, Zagorac S, Krell J, de Giorgio A, Trabulo SM, Nguyen VTM, Magnani L, Feng H et al. 2018. TGF-beta induces miR-100 and miR-125b but blocks let-7a through LIN28B controlling PDAC progression. *Nature communications* **9**: 1845.

Peng B, Theng PY, Le MTN. 2021. Essential functions of miR-125b in cancer. *Cell Prolif* **54**: e12913.

Peng Y, Croce CM. 2016. The role of MicroRNAs in human cancer. *Signal Transduction and Targeted Therapy* **1**: 15004.

Qin C, Huang RY, Wang ZX. 2015. Potential role of miR-100 in cancer diagnosis, prognosis, and therapy. *Tumour Biol* **36**: 1403-1409.

Schossleitner K, Rauscher S, Groger M, Friedl HP, Finsterwalder R, Habertheuer A, Sibilia M, Brostjan C, Fodinger D, Citi S et al. 2016. Evidence That Cingulin Regulates Endothelial Barrier Function In Vitro and In Vivo. *Arterioscler Thromb Vasc Biol* **36**: 647-654.

Skog J, Würdinger T, Rijn Sv, Meijer DH, Gainche L, Jr WTC, Carter BS, Krichevsky AM, Breakefield XO. 2008. Glioblastoma microvesicles transport RNA and proteins that promote tumour growth and provide diagnostic biomarkers. *Nature Cell Biology* **10**: 1470.

Subramanian A, Tamayo P, Mootha VK, Mukherjee S, Ebert BL, Gillette MA, Paulovich A, Pomeroy SL, Golub TR, Lander ES et al. 2005. Gene set enrichment analysis: a knowledge-based approach for interpreting genome-wide expression profiles. *Proc Natl Acad Sci U S A* **102**: 15545-15550.

Valadi H, Ekstrom K, Bossios A, Sjostrand M, Lee JJ, Lotvall JO. 2007. Exosome-mediated transfer of mRNAs and microRNAs is a novel mechanism of genetic exchange between cells. *Nat Cell Biol* **9**: 654-659.

Vickers KC, Palmisano BT, Shoucri BM, Shamburek RD, Remaley AT. 2011. MicroRNAs are transported in plasma and delivered to recipient cells by high-density lipoproteins. *Nat Cell Biol* **13**: 423-433.

Wang J, Vasaikar S, Shi Z, Greer M, Zhang B. 2017. WebGestalt 2017: a more comprehensive, powerful, flexible and interactive gene set enrichment analysis toolkit. *Nucleic Acids Res* **45**: W130-W137.

Zhang X, Li T, Han YN, Ge M, Wang P, Sun L, Liu H, Cao T, Nie Y, Fan D et al. 2021. miR-125b Promotes Colorectal Cancer Migration and Invasion by Dual-Targeting CFTR and CGN. *Cancers (Basel)* **13**.

Zhao S, Guo Y, Sheng Q, Shyr Y. 2014. Advanced heat map and clustering analysis using heatmap3. *BioMed research international* **2014**: 986048.

## Figure Legends

**Figure 1. Gene expression levels of miR-100 and miR-125b in CC, CC-CR and Δ miR-100/miR-125b.** (A) The 115kb *MIR100HG* is a host gene to lnc MIR100HG (3kb), miRNAs (miR-100, miR-125b, let-7a) and a protein coding region (BLID). In CC-CR cells, lncMIR100HG, miR-100 and miR-125b are highly expressed, while let-7a is not. (B) RT-qPCR analysis of miR-100 and miR-125b expression in comparison CC and CC-CR cells. (C) RT-qPCR analysis of miR-100 and miR-125b in CC-CR cells and CC-CR cells that have had miR-100, miR-125b, or both miR-100 and miR-125b knocked out by CRIPSR-Cas9. Fold changes for RT-qPCR were determined using ΔΔC(t) method. ** indicates a p-value of <0.005 and **** indicates a p-value of <0.0001.

**Figure 2. Identification of potential mRNA target of miR-100 and miR-125b in colorectal cancer cells.** Two different methods were used to find a total of 117 potential mRNA targets of miR-100 and miR-125b. (A) Schematic of first method for identifying potential mRNA targets of miR-100 and miR-125b. Individual miRNA and dual miRNA knockouts were created then RNA was collected and send for RNAseq. A heatmap for potential targets that are upregulated in CC cells (>2 fold), upregulated in knockout cells (>1.5 fold), and are canonical targets based on target prediction algorithms are shown (B). A schematic for the second method of identifying targets of miR-100 and miR-125b is shown (C). RNA collected from Ago2-RIP from CC and CC-CR cells was analyzed for potential targets that were associated with Ago2 in CC-CR cells but not in CC cells. These potential targets were then compared to mRNAs that are upregulated in CC cells (>2 fold), upregulated in knockout cells (>1.5 fold). (D) A heatmap of potential targets are shown based on gene expression in the knockout cells.

**Figure 3. miR-100 and miR-125b target a variety of mRNAs in colorectal cancer cells.** (A) Luciferase plasmids were generated to test miR-100 and miR-125b binding in high miR-100 and miR-125b expressing (CC-CR) cells and Δ miR-100/miR-125b. Empty plasmids are luciferase plasmids with no 3'UTR added into the vector. 100 and 125 vectors are two different vectors that have either three prefect binding sites for miR-100 or miR-125b, respectively. The experimental vectors were generated to have the 3'UTR of one of the potential targets acting as the 3'UTR for the luciferase. (B) Quantification of relative luciferase after transfection of the indicated luciferase plasmid are shown. Relative luciferase was calculated by normalizing to co-transfected internal control (Renilla vector), then calculating luciferase value for experimental vector/ luciferase

value for empty vector. * indicates a p-value <0.05, ** indicates a p-value < 0.01, *** indicates a p-value <0.001, **** indicates a p-value <0.0001.

**Figure 4. Cingulin and PTPRR expression levels within various cancer cells and corresponding normal tissue.** (A) A boxplot of CGN expression across 72 paired tissues in GPL570 platform. Red indicates cancer samples, while blue indicates normal samples. CGN expression is significantly downregulated in colon cancer compared to normal (t-test, p<0.001,log2FC=-1.13). (B) A boxplot of PTPRR expression across 72 paired tissues in GPL570 platform. Red indicates cancer samples, while blue indicates normal samples. PTPRR expression is significantly downregulated in colon cancer compared to normal (t-test, p<0.001,log2FC=-1.618).

**Figure 5. miR-100 and miR-125b functionally transfer through extracellular communication in colorectal cancer cells.** (A) RNA was collected from EVs from CC and CC-CR cells and RT-qPCR analysis was completed using the ΔΔC(t) method. (B) Recipient ΔmiR-100/miR-125b cells were cultured in Transwell with indicated donor cells (ΔmiR-100/miR-125b or CC-CR). RNA was collected from the recipient cells and RT-qPCR analysis was completed using the ΔΔC(t) method. (C) Schematic of work-flow of functional transfer assay. (D)ΔmiR-100/miR-125b were plated as recipient cells while the donor cells are either ΔmiR-100/miR-125b (Grey) or CC-CR (Black) cells. Relative luciferase value for the indicated luciferase vector was calculated normalizing to co-transfected internal control (Renilla vector), then calculating luciferase value for experimental vector/ luciferase value for empty vector. * indicates a p-value <0.05, ** indicates a p-value < 0.01, *** indicates a p-value <0.001, **** indicates a p-value <0.0001, and ns is not significant.

**Figure 6. CGN expression decreases with increased miR-100 and miR-125b at cell contact site by immunofluorescence in colorectal cancer cells.** (A) Immunofluorescence of nuclei (blue), F-actin (green), and CGN (white), with a composite image for the indicated cell types. (B) Immunofluorescence of nuclei (blue), F-actin (green), and CGN (white), with a composite image for the recipient ΔmiR-100/miR-125b co-cultured in transwell with the indicated cell types.

**Figure 7. Spheroid growth phenotypes are altered by miR-100 and miR-125b levels in colorectal cancer.** (A) Spheroids of indicated cell types were plated in collagen on Day 0 and imaged for 5 days. (B) Area increase was determined by measuring the surface area of the spheroid on Day 0/ Day5. Surface area tracing completed in ImageJ is shown in yellow. (C) Projection surface area was calculated from taking the total surface area (yellow) and subtracting the surface area of the main spheroid (red). ** indicates a p-value < 0.01, *** indicates a p-value <0.001, ns is not significant.

**Supplemental Table 1. Primers used to generate luciferase plasmid assay vectors.** Table showing the name of the vector and the primers used to clone the perfect binding sites for the miRNAs or the 3'UTR of the mRNA of interest.

**Supplemental Table 2. Long RNAseq data from ΔmiR-100, ΔmiR-125b, and ΔmiR-100/miR-125b compared to CC-CR cells.** Sequencing data for libraries generated from RNA >200nt isolated from the multiple knockout cell lines generated. Long RNAseq data sets are represented by different tabs within the file. Significant differentially expressed genes with absolute fold change > 2 or < 0.5, and adjusted p values (padj) <0.05 were determined using DESeq2 (v1.30.1)(Love et al. 2014).

**Supplemental Table 3. Small RNAseq data from Ago2 RNA immunoprecipitation from CC and CC-CR cells.** Sequencing data for libraries generated from RNA <200nt isolated CC and CC-CR cells, as well as RNA isolated from Ago2 RNA immunoprecipitation. Small RNAseq data sets are represented by different tabs within the file. Significant differentially expressed genes with absolute fold change > 2 or < 0.5, and adjusted p values (padj) <0.05 were determined using DESeq2 (v1.30.1)(Love et al. 2014).

**Supplemental Table 4. Long RNAseq data from Ago2 RNA immunoprecipitation from CC and CC-CR cells.** Sequencing data for libraries generated from RNA >200nt isolated from CC and CC-CR cells, as well as RNA isolated from Ago2 RNA immunoprecipitation. Long RNAseq data sets are represented by different tabs within the file. Significant differentially expressed genes with absolute fold change > 2 or < 0.5, and adjusted p values (padj) <0.05 were determined using DESeq2 (v1.30.1)(Love et al. 2014).

**Supplemental Figure 1. Schematic of ΔmiR-100, ΔmiR-125b, and ΔmiR-100/miR-125b CC-CR cells.** CRISPR cas9 (scissors) was used to generate the different knockout cell lines. The use of different gRNAs generated the genotypes that are illustrated.

**Supplemental Figure 2. Quality control of long RNAseq from Ago2 RNA immunoprecipitation.** RNAseq was performed in triplicate on RNA (<200nt) isolated from CC and CC-CR cells, as well as RNA isolated from Ago2 RNA immunoprecipitation. Read numbers and percentage of reads mapping to the categories indicated at the top are as shown.

**Supplemental Figure 3. Differential expression of long RNAs from Ago2 RNA immunoprecipitation.** (A) Volcano plot showing up- and down-regulated long RNA in CC and CC-CR cell lysate. (B)Volcano plot showing up- and down-regulated long RNA from Ago2 immunoprecipitation from CC and CC-CR cells.

**Supplemental Figure 4. miR-100 and miR-125b binds to all eight verified mRNA targets.** All targets that have were verified by the luciferase screen are shown. Each mRNA is shown with a coding region (green), followed by the 3' UTR. The mRNA is labeled so that the length of the 3'UTR is shown. The binding sites for miR-100 (red) and miR-125b (blue) are shown for the mRNA and the seed sequence of the miRNA. The solid lines indicate potential direct binding sites within the seed sequence; dotted

lines indicate potential binding sites outside of the seed sequence of the miRNA that enhances binding potential.

**Supplemental Movie 1. Timelapse movie of ΔmiR-100/miR-125b spheroid growing.** ΔmiR-100/miR-125b spheroids were grown in collagen with images taken every hour for five days. The movie shows seven still pictures (taken over seven hours) per second.

**Supplemental Movie 2. Timelapse movie of CC spheroid growing.** CC spheroids were grown in collagen with images taken every hour for five days. The movie shows seven still pictures (taken over seven hours) per second.

**Supplemental Movie 3. Timelapse movie of CC-CR spheroid growing.** CC-CR spheroids were grown in collagen with images taken every hour for five days. The movie shows seven still pictures (taken over seven hours) per second.

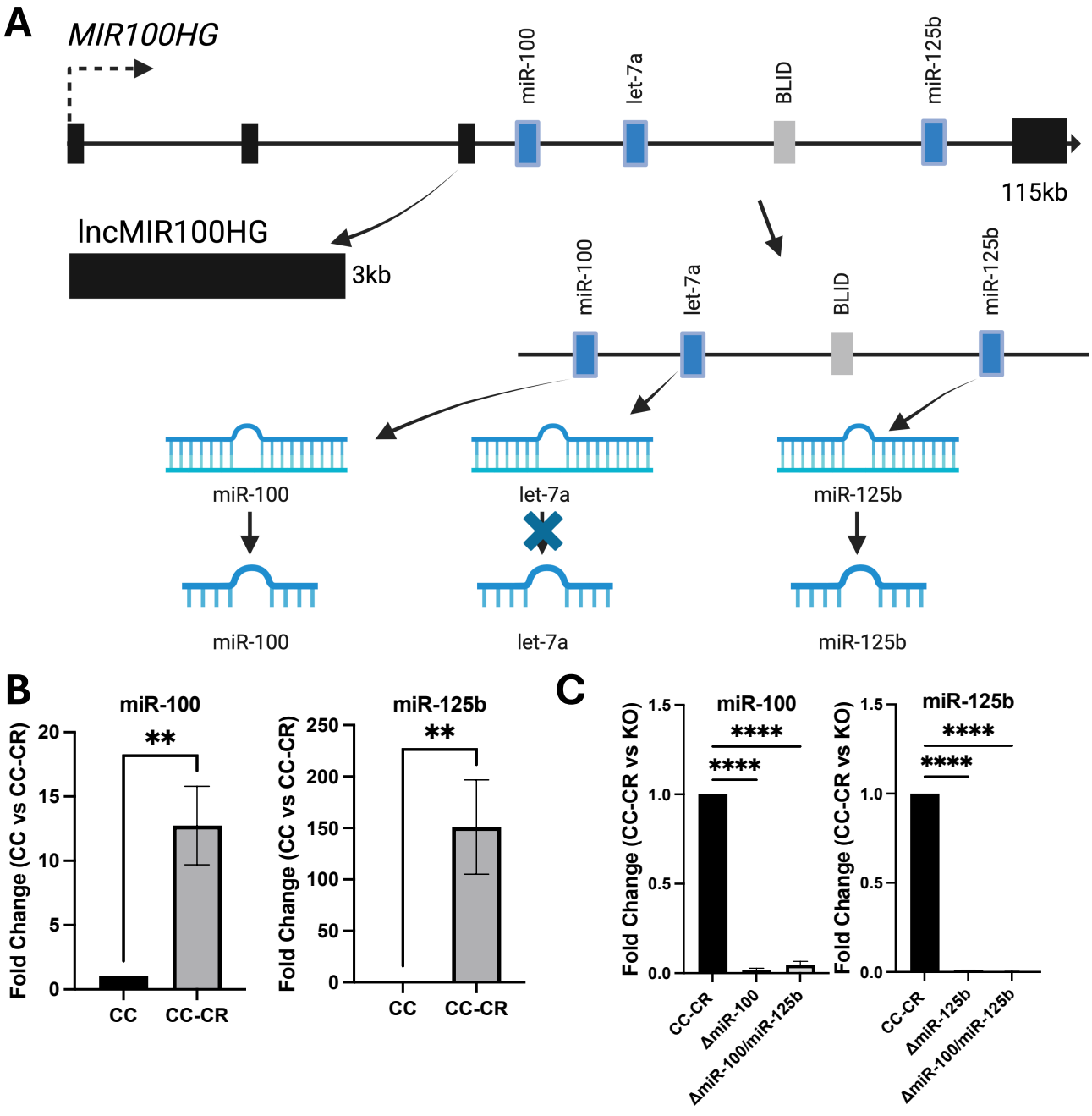
A
MIR100HG
miR-100
let-7a
BLID
miR-125b
115kb
lncMIR100HG
3kb
miR-100
let-7a
BLID
miR-125b
miR-100
let-7a
miR-125b
miR-100
let-7a
miR-125b
B
miR-100
Fold Change (CC vs CC-CR)
20
15
10
5
0
**
CC
CC-CR
miR-125b
Fold Change (CC vs CC-CR)
250
200
150
100
50
0
**
CC
CC-CR
C
miR-100
Fold Change (CC-CR vs KO)
1.5
1.0
0.5
0.0
****
****
CC-CR
ΔmiR-100
ΔmiR-100/miR-125b
miR-125b
Fold Change (CC-CR vs KO)
1.5
1.0
0.5
0.0
****
****
CC-CR
ΔmiR-125b
ΔmiR-100/miR-125b

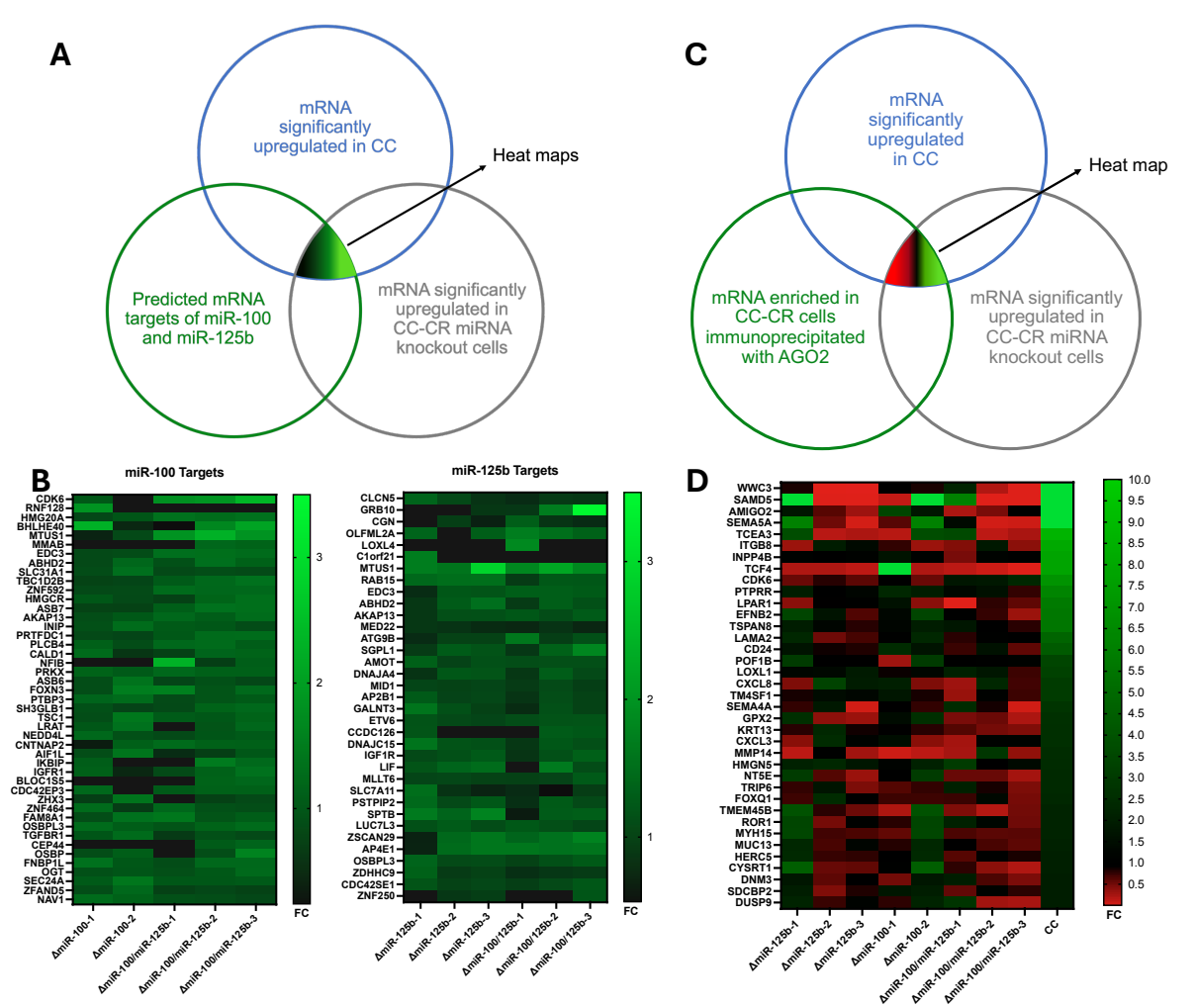
A
mRNA significantly upregulated in CC
Heat maps
Predicted mRNA targets of miR-100 and miR-125b
mRNA significantly upregulated in CC-CR miRNA knockout cells
C
mRNA significantly upregulated in CC
Heat map
mRNA enriched in CC-CR cells immunoprecipitated with AGO2
mRNA significantly upregulated in CC-CR miRNA knockout cells
B
miR-100 Targets
CDK6
RNF128
HMG20A
BHLHE40
MTUS1
MMAB
EDC3
ABHD2
SLC31A1
TBC1D2B
ZNF592
HMGCR
ASB7
AKAP13
INIP
PRTFDC1
PLCB4
CALD1
NFIB
PRKX
ASB6
FOXN3
PTBP3
SH3GLB1
TSC1
LRAT
NEDD4L
CNTNAP2
AIF1L
IKBIP
IGFR1
BLOC1S5
CDC42EP3
ZHX3
ZNF464
FAM8A1
OSBPL3
TGFBR1
CEP44
OSBP
FNBP1L
OGT
SEC24A
ZFAND5
NAV1
3
2
1
FC
ΔmiR-100-1
ΔmiR-100-2
ΔmiR-100/miR-125b-1
ΔmiR-100/miR-125b-2
ΔmiR-100/miR-125b-3
miR-125b Targets
CLCN5
GRB10
CGN
OLFML2A
LOXL4
C1orf21
MTUS1
RAB15
EDC3
ABHD2
AKAP13
MED22
ATG9B
SGPL1
AMOT
DNAJA4
MID1
AP2B1
GALNT3
ETV6
CCDC126
DNAJC15
IGF1R
LIF
MLLT6
SLC7A11
PSTPIP2
SPTB
LUC7L3
ZSCAN29
AP4E1
OSBPL3
ZDHHC9
CDC42SE1
ZNF250
3
2
1
FC
ΔmiR-125b-1
ΔmiR-125b-2
ΔmiR-125b-3
ΔmiR-100/125b-1
ΔmiR-100/125b-2
ΔmiR-100/125b-3
D
WWC3
SAMD5
AMIGO2
SEMA5A
TCEA3
ITGB8
INPP4B
TCF4
CDK6
PTPRR
LPAR1
EFNB2
TSPAN8
LAMA2
CD24
POF1B
LOXL1
CXCL8
TM4SF1
SEMA4A
GPX2
KRT13
CXCL3
MMP14
HMGN5
NT5E
TRIP6
FOXQ1
TMEM45B
ROR1
MYH15
MUC13
HERC5
CYSRT1
DNM3
SDCBP2
DUSP9
10.0
9.5
9.0
8.5
8.0
7.5
7.0
6.5
6.0
5.5
5.0
4.5
4.0
3.5
3.0
2.5
2.0
1.5
1.0
0.5
FC
ΔmiR-125b-1
ΔmiR-125b-2
ΔmiR-125b-3
ΔmiR-100-1
ΔmiR-100-2
ΔmiR-100/miR-125b-1
ΔmiR-100/miR-125b-2
ΔmiR-100/miR-125b-3
CC

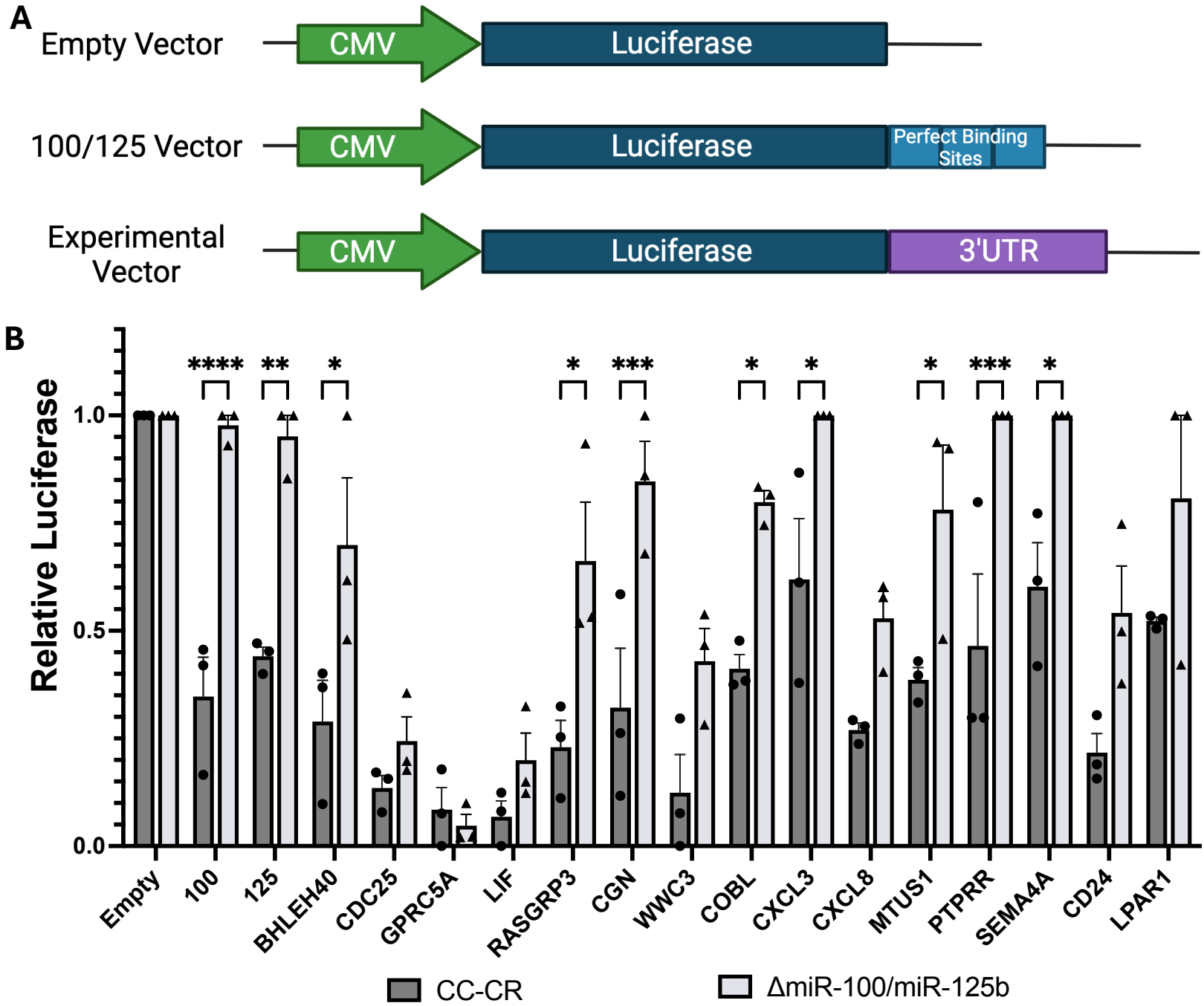
A
Empty Vector
CMV
Luciferase
100/125 Vector
CMV
Luciferase
Perfect Binding Sites
Experimental Vector
CMV
Luciferase
3'UTR
B
Relative Luciferase
1.0
0.5
0.0
****
**
*
*
***
*
*
*
***
*
Empty
100
125
BHLEH40
CDC25
GPRC5A
LIF
RASGRP3
CGN
WWC3
COBL
CXCL3
CXCL8
MTUS1
PTPRR
SEMA4A
CD24
LPAR1
CC-CR
ΔmiR-100/miR-125b

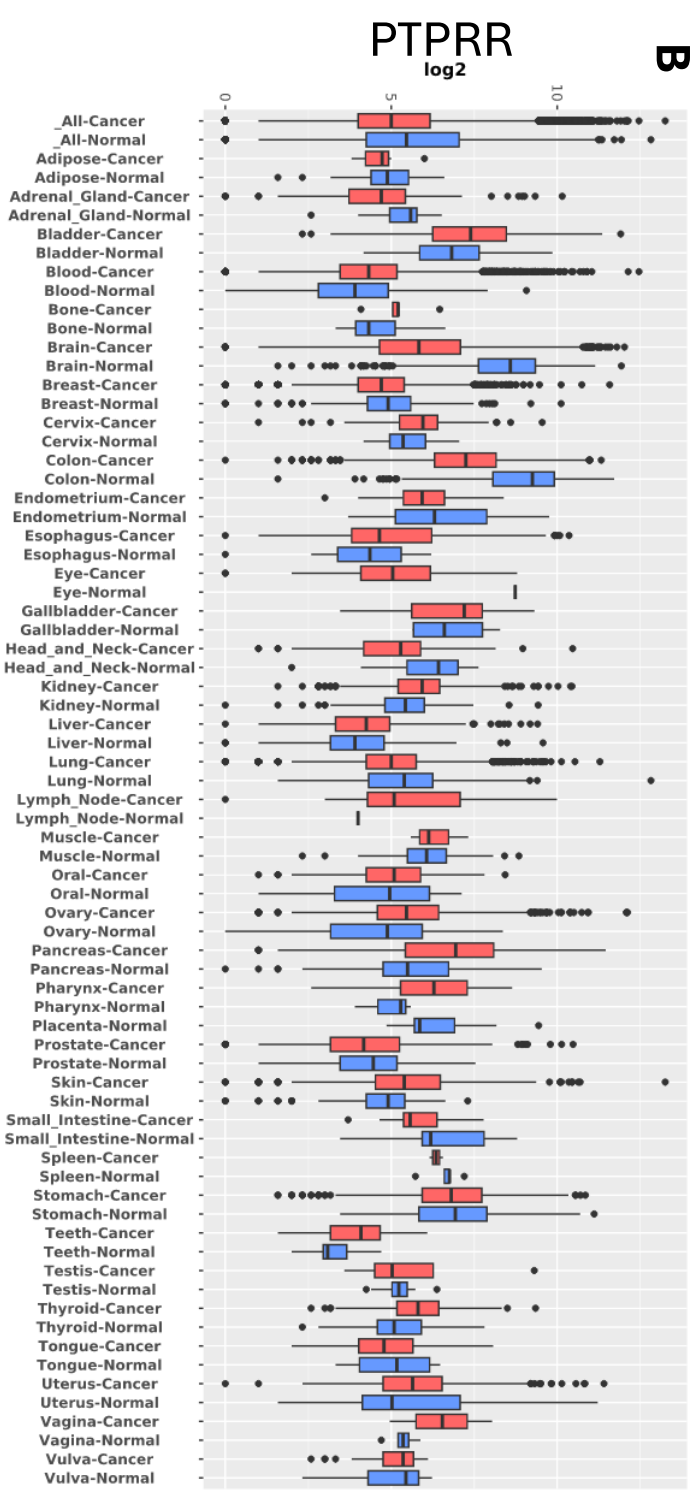
PTPRR
log2
B
0
5
10
_All-Cancer
_All-Normal
Adipose-Cancer
Adipose-Normal
Adrenal_Gland-Cancer
Adrenal_Gland-Normal
Bladder-Cancer
Bladder-Normal
Blood-Cancer
Blood-Normal
Bone-Cancer
Bone-Normal
Brain-Cancer
Brain-Normal
Breast-Cancer
Breast-Normal
Cervix-Cancer
Cervix-Normal
Colon-Cancer
Colon-Normal
Endometrium-Cancer
Endometrium-Normal
Esophagus-Cancer
Esophagus-Normal
Eye-Cancer
Eye-Normal
Gallbladder-Cancer
Gallbladder-Normal
Head_and_Neck-Cancer
Head_and_Neck-Normal
Kidney-Cancer
Kidney-Normal
Liver-Cancer
Liver-Normal
Lung-Cancer
Lung-Normal
Lymph_Node-Cancer
Lymph_Node-Normal
Muscle-Cancer
Muscle-Normal
Oral-Cancer
Oral-Normal
Ovary-Cancer
Ovary-Normal
Pancreas-Cancer
Pancreas-Normal
Pharynx-Cancer
Pharynx-Normal
Placenta-Normal
Prostate-Cancer
Prostate-Normal
Skin-Cancer
Skin-Normal
Small_Intestine-Cancer
Small_Intestine-Normal
Spleen-Cancer
Spleen-Normal
Stomach-Cancer
Stomach-Normal
Teeth-Cancer
Teeth-Normal
Testis-Cancer
Testis-Normal
Thyroid-Cancer
Thyroid-Normal
Tongue-Cancer
Tongue-Normal
Uterus-Cancer
Uterus-Normal
Vagina-Cancer
Vagina-Normal
Vulva-Cancer
Vulva-Normal

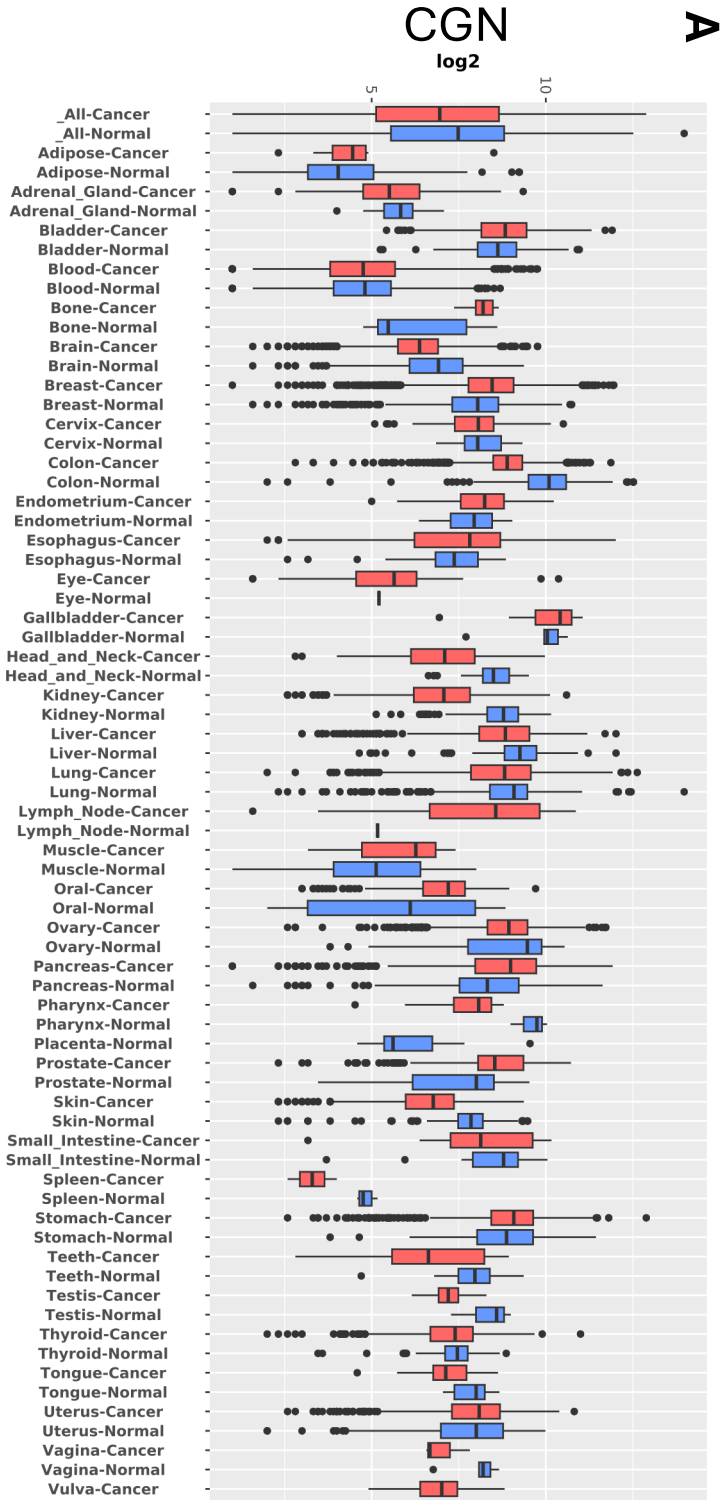
CGN
log2
A
5
10
_All-Cancer
_All-Normal
Adipose-Cancer
Adipose-Normal
Adrenal_Gland-Cancer
Adrenal_Gland-Normal
Bladder-Cancer
Bladder-Normal
Blood-Cancer
Blood-Normal
Bone-Cancer
Bone-Normal
Brain-Cancer
Brain-Normal
Breast-Cancer
Breast-Normal
Cervix-Cancer
Cervix-Normal
Colon-Cancer
Colon-Normal
Endometrium-Cancer
Endometrium-Normal
Esophagus-Cancer
Esophagus-Normal
Eye-Cancer
Eye-Normal
Gallbladder-Cancer
Gallbladder-Normal
Head_and_Neck-Cancer
Head_and_Neck-Normal
Kidney-Cancer
Kidney-Normal
Liver-Cancer
Liver-Normal
Lung-Cancer
Lung-Normal
Lymph_Node-Cancer
Lymph_Node-Normal
Muscle-Cancer
Muscle-Normal
Oral-Cancer
Oral-Normal
Ovary-Cancer
Ovary-Normal
Pancreas-Cancer
Pancreas-Normal
Pharynx-Cancer
Pharynx-Normal
Placenta-Normal
Prostate-Cancer
Prostate-Normal
Skin-Cancer
Skin-Normal
Small_Intestine-Cancer
Small_Intestine-Normal
Spleen-Cancer
Spleen-Normal
Stomach-Cancer
Stomach-Normal
Teeth-Cancer
Teeth-Normal
Testis-Cancer
Testis-Normal
Thyroid-Cancer
Thyroid-Normal
Tongue-Cancer
Tongue-Normal
Uterus-Cancer
Uterus-Normal
Vagina-Cancer
Vagina-Normal
Vulva-Cancer
Vulva-Normal

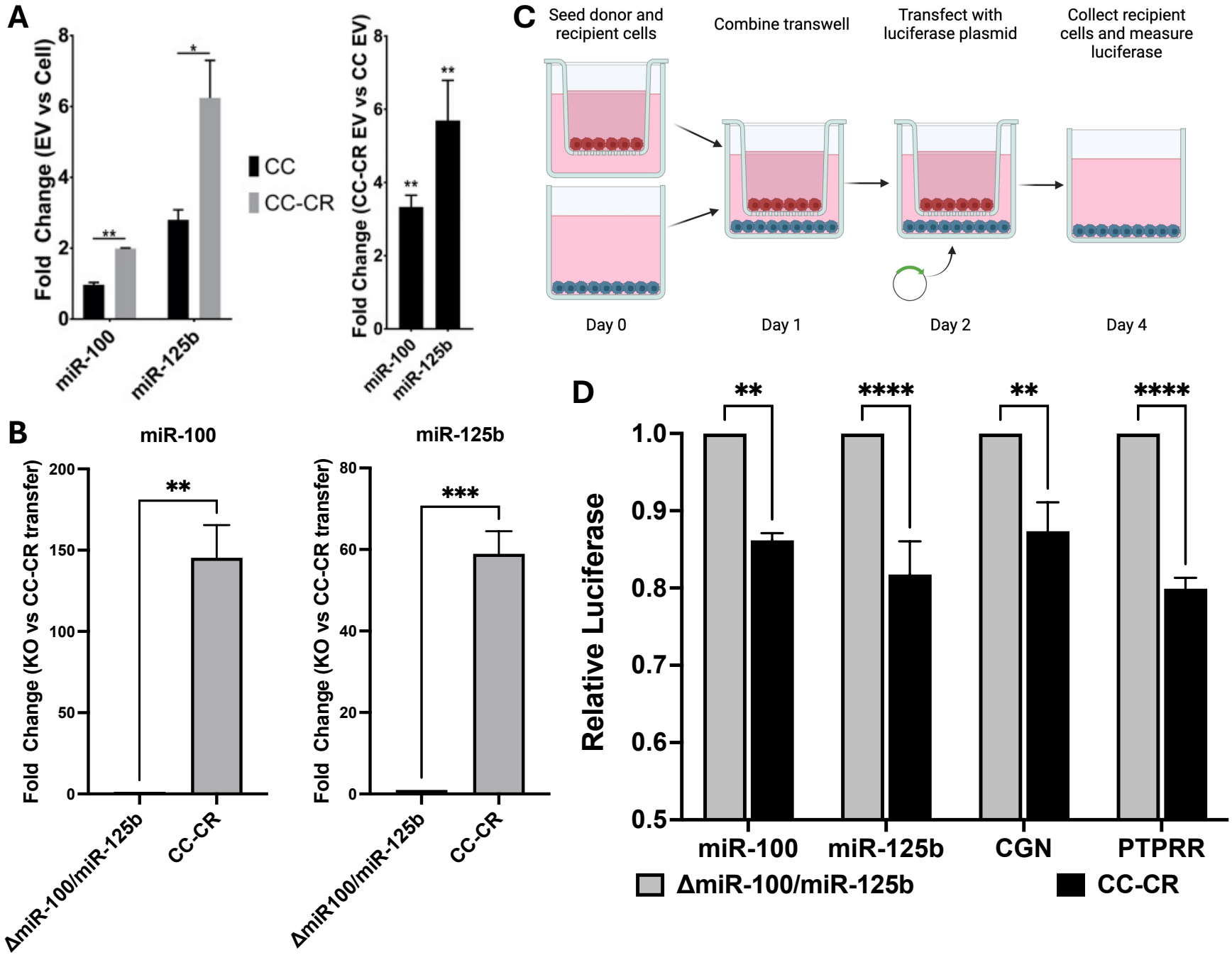
A
Fold Change (EV vs Cell)
CC
CC-CR
miR-100
miR-125b
Fold Change (CC-CR EV vs CC EV)
B
miR-100
miR-125b
Fold Change (KO vs CC-CR transfer)
ΔmiR-100/miR-125b
CC-CR
ΔmiR100/miR-125b
C
Seed donor and recipient cells
Combine transwell
Transfect with luciferase plasmid
Collect recipient cells and measure luciferase
Day 0
Day 1
Day 2
Day 4
D
Relative Luciferase
miR-100
miR-125b
CGN
PTPRR
ΔmiR-100/miR-125b
CC-CR

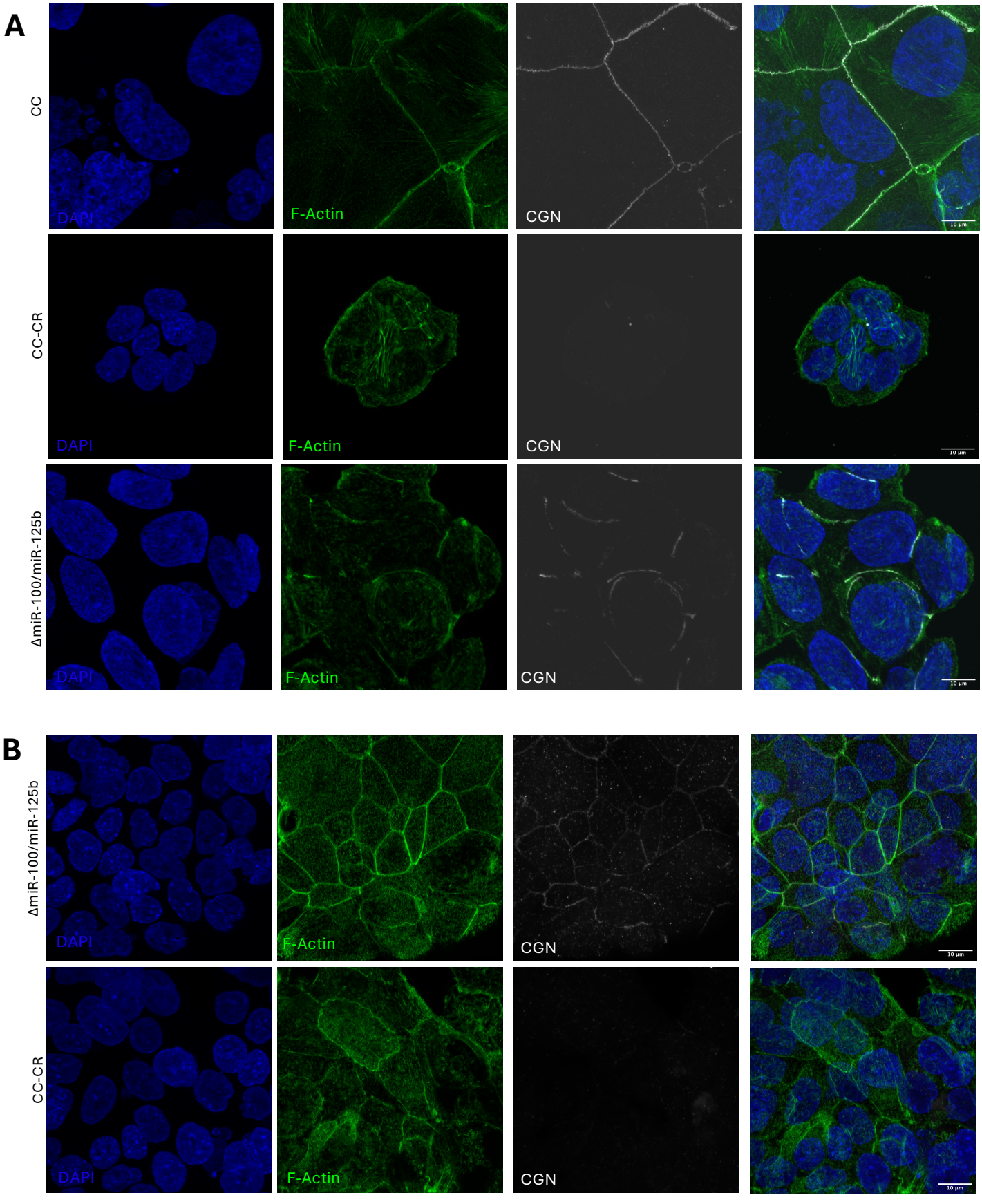
A
CC
CC-CR
ΔmiR-100/miR-125b
DAPI
F-Actin
CGN
B
ΔmiR-100/miR-125b
CC-CR
DAPI
F-Actin
CGN

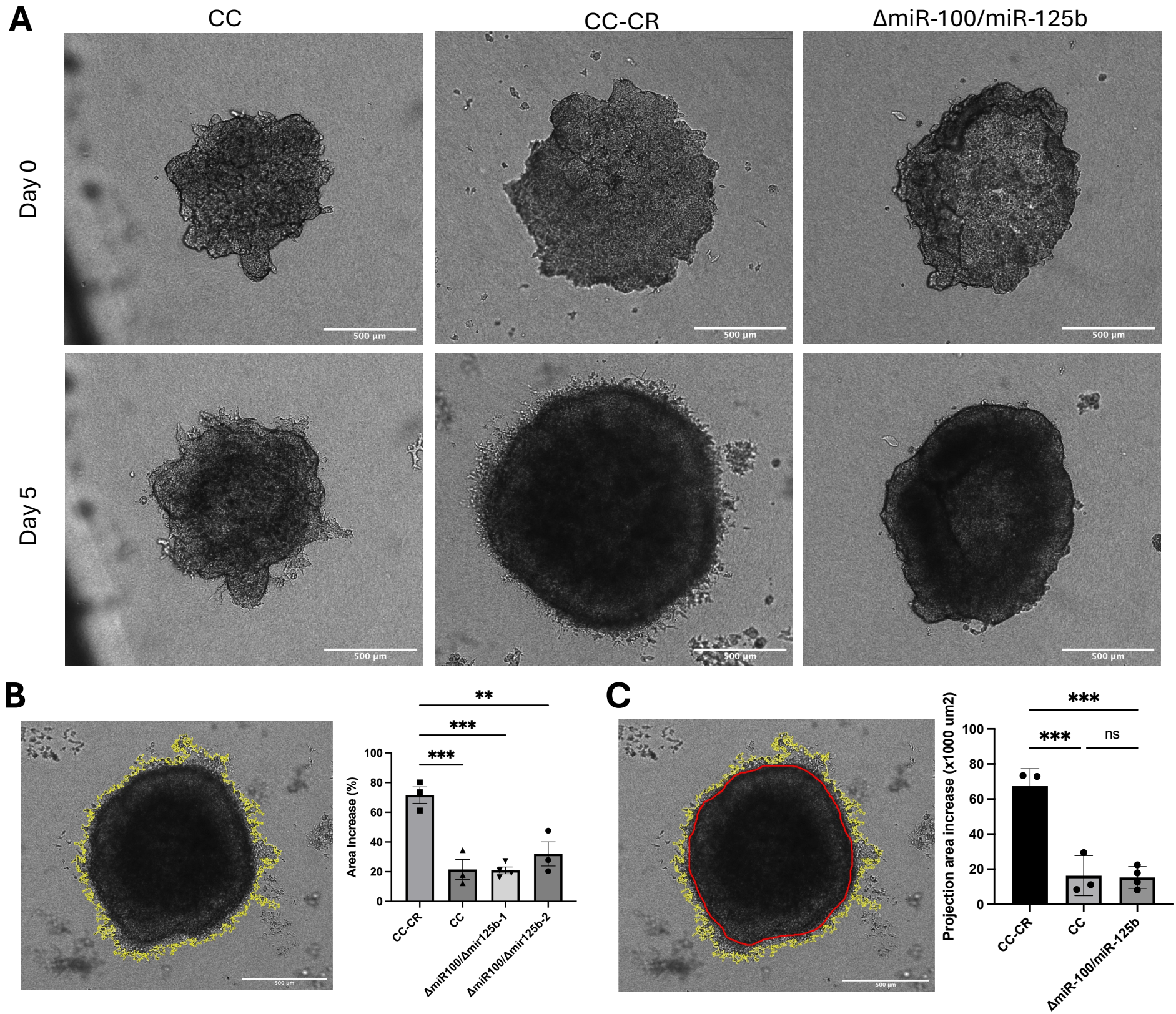
A
CC
CC-CR
ΔmiR-100/miR-125b
Day 0
Day 5
500 µm
B
Area Increase (%)
100
80
60
40
20
0
***
***
**
CC-CR
CC
ΔmiR100/Δmir125b-1
ΔmiR100/Δmir125b-2
C
Projection area increase (x1000 um2)
100
80
60
40
20
0
***
***
ns
CC-CR
CC
ΔmiR-100/miR-125b